JCB Article

Mutations in *sticky* lead to defective organization of the contractile ring during cytokinesis and are enhanced by *Rho* and suppressed by *Rac*

Pier Paolo D'Avino, Matthew S. Savoian, and David M. Glover

Cancer Research UK Cell Cycle Genetics Research Group, Department of Genetics, University of Cambridge, Cambridge CB2 3EH, UK

The contractile ring is a highly dynamic structure, but how this dynamism is accomplished remains unclear. Here, we report the identification and analysis of a novel *Drosophila* gene, *sticky (sti)*, essential for cytokinesis in all fly proliferating tissues. *sti* encodes the *Drosophila* orthologue of the mammalian Citron kinase. RNA interference–mediated silencing of *sti* in cultured cells causes them to become multinucleate. Components of the contractile ring and central spindle are recruited normally in such STICKY-depleted cells that nevertheless display asymmetric furrowing and aberrant blebbing. Together with an unusual distribution of F-actin and Anillin, these phenotypes are consistent with defective organization of the contractile ring. *sti* shows opposite genetic interactions with *Rho* and *Rac* genes suggesting that these GTPases antagonistically regulate STICKY functions. Similar genetic evidence indicates that RacGAP50C inhibits Rac during cytokinesis. We discuss that antagonism between Rho and Rac pathways may control contractile ring dynamics during cytokinesis.

Introduction

The finely orchestrated process of cytokinesis requires the formation and ingression of a cleavage furrow generated by the constriction of an actomyosin contractile ring anchored to the cell membrane by cytoskeletal proteins (Glotzer, 2001). Several studies in different systems clearly indicate that an array of antiparallel and interdigitating microtubules known as the central spindle plays a crucial role during both cleavage furrow formation and ingression (Field et al., 1999). Despite the identification of several gene products essential for central spindle and contractile ring formation, the signals that control cytokinesis remain poorly understood. A growing body of data suggests that the Rho family of small GTPases, known to control cytoskeletal rearrangements in all eukaryotes, orchestrate both the assembly and the contractility of the actomyosin ring (Prokopenko et al., 2000). Rho GTPases act as molecular switches cycling from an inactive (GDP bound) to active (GTP bound) state. The concentration of active and inactive forms is controlled by guanine nucleotide exchange factors (GEFs) that promote GTP binding, and GTPase activating proteins (GAPs) that promote GTP hydrolysis. The roles of the different Rho family members, Rho, Rac, and Cdc42, in controlling cytokinesis are not fully understood. RhoA seems to be a key regulator, as its inactivation by mutation, drug treatment, or RNA interference (RNAi) blocks cytokinesis in all systems investigated so far (Drechsel et al., 1997; O'Connell et al., 1999; Prokopenko et al., 1999; Somma et al., 2002). Moreover, the *Drosophila* RhoGEF PEBBLE and its mammalian orthologue ECT2 are also required for cleavage furrow ingression, supporting the idea that Rho activation is crucial for cytokinesis (Prokopenko et al., 1999; Tatsumoto et al., 1999). A conserved RacGAP, named CYK-4 in *C. elegans*, RacGAP50C in *Drosophila*, and MgcRacGAP in mammals, has also been shown to be essential for central spindle formation and cytokinesis (Jantsch-Plunger et al., 2000; Kitamura et al., 2001; Somers and Saint, 2003). This GAP appears to perform multiple functions during cytokinesis, some of which have yet to be completely defined. This protein localizes to

The online version of this article contains supplemental material.

Address correspondence to P.P. D'Avino or D.M. Glover, Department of Genetics, Downing Site, Cambridge, CB2 3EH, UK. Tel.: 44-1223-76-6739. Fax: 44-1223-33-3968. email: p.davino@gen.cam.ac.uk; or d.glover@gen.cam.ac.uk

Key words: cytokinesis; contractile ring; Citron kinase; Rho GTPases; *Drosophila*

Abbreviations used in this paper: CIT-K, Citron kinase; GAP, GTPase activating protein; GEF, guanine nucleotide exchange factor; MRLC, myosin regulatory light chain; PH, pleckstrin homology; RFLP, restriction fragment length polymorphism; RNAi, RNA interference; ROK, Rho kinase; *sqh*, *spaghetti squash*; *sti*, *sticky*.

The Journal of Cell Biology, Volume 166, Number 1, July 5, 2004 61–71
http://www.jcb.org/cgi/doi/10.1083/jcb.200402157

The Journal of Cell Biology

the central spindle and contractile ring and binds the ZEN-4/PAV/MKLP-1 kinesin-like protein to form an evolutionary conserved complex, named centralspindlin, able to bundle microtubules in vitro (Mishima et al., 2002; Somers and Saint, 2003). In addition, Somers and Saint (2003) have shown that RacGAP50C interacts synergistically with the RhoGEF PEBBLE to promote Rho activity during cytokinesis. Finally, although this RacGAP has been found in vitro to target Rac and Cdc42 more efficiently than Rho (Toure et al., 1998; Jantsch-Plunger et al., 2000), Minoshima et al. (2003) have recently proposed that phosphorylation by Aurora-B kinase converts MgcRacGAP to an RhoGAP during the final stages of cytokinesis.

RhoA can control both the assembly and the contractility of the actomyosin ring using different pathways. RhoA may promote actin polymerization upon binding to members of the formin homology protein family, which have been shown to interact with profilin in mammalian cells (Watanabe et al., 1997). Consistent with this, mutations in profilin and formin homology protein genes cause abortion of cytokinesis in *Drosophila* and *C. elegans* (Castrillon and Wasserman, 1994; Swan et al., 1998). RhoA also controls myosin II activity through its effector Rho kinase (ROK), which can phosphorylate the myosin regulatory light chain (MRLC; Amano et al., 1996; Winter et al., 2001). Genetic evidence in *Drosophila* clearly indicates that MRLC and its phosphorylation status are important for cytokinesis (Jordan and Karess, 1997). Both genetic and pharmacological studies indicate that ROK is involved in cytokinesis, even though this kinase may play a facilitating and not essential role in ring contraction (Kosako et al., 2000; Piekny and Mains, 2002). Another putative RhoA effector, Citron kinase (CIT-K) has recently been implicated in cytokinesis and proposed to regulate actomyosin contractility alternatively or redundantly to ROK (Madaule et al., 2000). CIT-K was initially identified in a two-hybrid screen for proteins interacting with RhoC and found to bind both RhoA and Rac, but not Cdc42 in vitro (Madaule et al., 1995). Subsequent results have implicated this gene in cytokinesis in mammalian cells (Madaule et al., 1998). Knockout mouse mutants, however, display cytokinesis defects only in some cell populations of the CNS and during spermatogenesis (Di Cunto et al., 2000, 2002). These latter results imply that CIT-K is not essential for cytokinesis in all tissues and challenge the idea that CIT-K is the major Rho effector controlling ring contractility.

Here, we describe the identification and analysis of a *Drosophila* gene, *sticky* (*sti*), required for cytokinesis in all postembryonic proliferating tissues. In *sti*-deficient cells, furrow ingression appears uncoordinated and is accompanied by dramatic blebbing with unusual accumulation and localization of F-actin and Anillin. *sti* encodes the *Drosophila* orthologue of CIT-K and its localization and behavior suggest that is its functional homologue. *sti* phenotypes are dominantly enhanced by *Rho* and suppressed by *Rac* genes, suggesting that its functions can be antagonistically regulated by these two GTPases. Similar genetic evidence also suggests that RacGAP50C inhibits Rac activity. Our observations suggest that Rac GTPases are down-regulated during cytokinesis and we discuss the possibility that antagonism between Rho and Rac signaling pathways controls contractile ring dynamics.

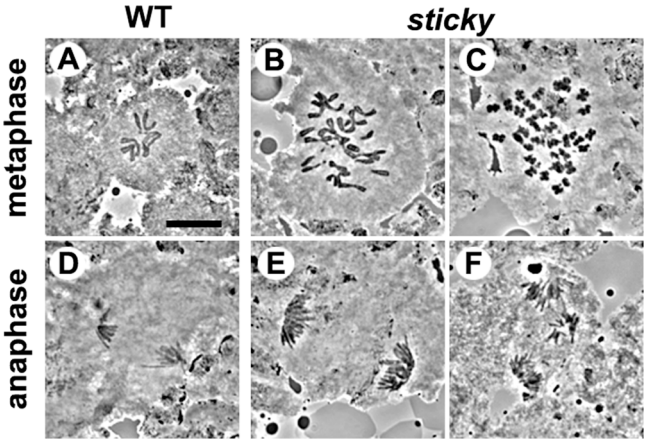

Figure 1. ***sti* mutant neuroblasts are polyploid.** Squashed preparations of third instar larval brains from wild-type (A and D, WT) and *sti* mutants (B, C, E, and F). A diploid wild-type (WT) metaphase and anaphase are shown in A and D, respectively. (B) A polyploid metaphase from a $sti^4/Df(3L)F10$ larva. (C) A polyploid metaphase containing hypercondensed chromosomes from a $sti^4/Df(3L)F10$ mutant. (E) A polyploid anaphase from a $sti^4/Df(3L)F10$ larva. (F) A polyploid, tripolar anaphase from a $sti^5/Df(3L)F10$ mutant larva. Bar, 10 μm.

Results

sti is required for cytokinesis

In a screen for *P* element–induced *Drosophila* mutants showing abnormal mitotic figures in neuroblasts of third instar larvae (Deak et al., 1997), we identified two different lines that displayed a polyploid phenotype consistent with a defect in cytokinesis (Fig. 1). These mutations were allelic to each other but the *P* elements were not responsible for the *sti* phenotypes (see next paragraph). The mutations were mapped to a region containing a gene, named *l(3)7m-62* or *sti* (see Materials and methods), that exhibits very similar mitotic defects (Gatti and Baker, 1989). Complementation analysis revealed that our mutants were allelic to *sti* and thus named sti^4 and sti^5. The mitotic index of *sti* mutants is very similar to that of wild-type larvae (Table I), suggesting a primary defect in cytokinesis. Moreover, the majority of polyploid neuroblasts exhibit normal chromosomes (Fig. 1, B, E, and F; Table I), indicating that sister chromatids segregated normally. Only a small fraction of cells showed hypercondensed chromosomes characteristic of karyokinesis defects (Table I; Fig. 1 C). However, these cells were also highly polyploid (8N or more), suggesting that defects in chromosome segregation are a secondary effect due to the presence of supernumerary centrosomes and consequent multipolar spindles (Fig. 1 E).

To evaluate each *sti* allele, we performed complementation and lethal stage analyses of all *sti* allelic combinations. We used a deficiency, *Df(3L)F10*, that completely removes the *sti* genomic region, and five different *sti* alleles (Table II). The sti^1 allele was originally described by Gatti and Baker (1989), sti^2 and sti^3 mutations were generated by chemical

Table I. **Mitotic activity and polyploidy in *sti* mutants**

Genotype	Brains/ microscope fields	MI	Anaphases	Polyploid cells				Hypercondensed
				4N	8N	>8N	Total	
OR-R	4/499	2.1	16.5	0	0	0	0	0
sti^{4}/*Df*	3/428	1.8	13.2	35.0	37.7	7.8	80.5	6.5
sti^{5}/*Df*	6/646	2.1	10.7	41.0	13.4	2.2	56.6	2.2
sti^{1}/*sti*^{4}	3/380	2.4	13.7	24.2	20.9	16.5	61.6	3.3
sti^{1}/*sti*^{5}	4/360	1.7	14.8	41.9	19.3	3.2	64.4	0
sti^{4}/*sti*^{5}	5/541	1.9	7.5	50.5	12.9	1.0	64.4	0

The deficiency strain (*Df*) used in these experiments is *Df(3L)F10* (see Materials and methods). The mitotic index (MI) is expressed as the number of mitotic cells per microscope field using a 60× objective and 1.6× intermediate lens. Anaphases are indicated as a percentage of all mitotic cells. 4N, 8N, and >8N indicate the percentage of cells displaying tetraploid, octaploid, or higher than octaploid chromosome content, respectively. The percentage of cells showing hypercondensed chromosomes is shown in the last column.

mutagenesis and *sti*^{4} and *sti*^{5} were isolated from the *P* element screen described above. The data shown in Table II reveal that in most homo- and heteroallelic combinations, *sti* mutants die at the onset of metamorphosis (prepupal stage, PP) because they have very small imaginal discs. This indicates that *sti* is essential for imaginal cell division. Lethal phase analysis showed that all *sti* alleles behave as hypomorphs with *sti*^{3} being the most severe and *sti*^{5} the weakest (Table II). All other alleles appeared to have similar strength.

sti encodes a serine/threonine kinase related to the mammalian CIT-K

Precise excisions of the *P* elements present in *sti*^{4} and *sti*^{5} mutants did not rescue either the lethality or the polyploidy observed in these animals (unpublished data), indicating that these elements were not inserted within the *sti* gene. Using both deficiency and recombination mapping we were able to map the *sti* gene to the 69D2-3 polytene region in an area uncovered by two deficiencies, *Df(3L)F10* and *Df(3L)E44*. Although the *P* elements were not inserted in the *sti* gene, we surmised that some rearrangements might have occurred in the genomes of these lines during the mutagenesis. Thus, we decided to look for possible RFLPs (restriction fragment length polymorphisms) in the genomic region uncovered by the two deficiencies in *sti*^{4} and *sti*^{5} mutants. As a starting point we used another gene studied in the lab, *vihar*, which also maps to the same region (unpublished data). In this way, we identified two RFLPs in two adjacent EcoRI fragments that harbor a single transcription unit, identified as CG10522 by the *Drosophila* genome project (Fig. 2 A; Celniker et al., 2002).The sequence of four different CG10522 cDNAs revealed a single ORF coding for a 1,854–amino acid protein of a predicted mass of 211 kD (Fig. 2 B). Northern blot analysis indicated that CG10522 encodes a single transcript of ~6.1 kb (Fig. 2 C) that is prematurely truncated (and slightly more abundant) in *sti*^{5} mutants and very unstable in *sti*^{4} animals. To further confirm that CG10522 is indeed *sti*, we sequenced its genomic region in all *sti* mutants and found two *hobo* transposable element insertions in *sti*^{4} and *sti*^{5} and three premature termination codons in *sti*^{1}, *sti*^{2}, and *sti*^{3} at residues 1093, 1126, and 348, respectively (Fig. 2 B). We also raised an antibody against the CG10522 protein and analyzed its expression in *sti* mutant larval brains by Western Blot. As shown in Fig. 2 D, this antibody recognizes a single product of ~220 kD, in good agreement with the CG10522 predicted molecular weight. This protein is truncated prematurely in *sti*^{1}, *sti*^{2}, and *sti*^{5} and undetectable in *sti*^{4}, exactly as predicted by sequence and Northern blot analysis (Fig. 2, B–D). Thus, CG10522 is the *sti* gene.

Table II. **Complementation and lethal phase analysis of *sti* alleles**

	Df(3L)F10	*sti*^{1}	*sti*^{2}	*sti*^{3}	*sti*^{4}	*sti*^{5}
Df(3L)F10	E	PP	PP	L3	PP	PP/P/PA/A
***sti*^{1}**		PP	PP	PP	PP	PA/A
***sti*^{2}**			ND	PP	PP	PA/A
***sti*^{3}**				ND	PP	PA/A
***sti*^{4}**					PP	PA/A
***sti*^{5}**						A/V (ms, frf)[a]

The lethal stages are indicated as follows: E, embryonic; L3, third larval instar (prewandering stage); PP, prepupal; P, pupal; PA, pharate adult; A, adult (flies are able to eclose from the pupal case but die soon thereafter); V, viable. At least 50 animals were analyzed for each genotype. The lethality of *sti*^{2} and *sti*^{3} homozygous animals could not be determined (ND) due to the presence of additional mutations on these chromosomes. All the animals that die at the prepupal stage have very small imaginal discs.
[a]In single pair mating experiments with wild-type opposites, all *sti*^{5} males analyzed were completely sterile (ms, male sterility), whereas some *sti*^{5} females were fertile (frf, female reduced fertility).

Database searches revealed that *sti* encodes a serine/threonine kinase closely related to the mammalian CIT-K (Madaule et al., 1995, 2000; Di Cunto et al., 1998). CIT-K and STICKY share several common functional and structural domains. The highest degree of identity lies in the kinase domain (44%), followed by the CitroN Homology domain (32%), a relatively novel motif of unclear function found in Citron and NIK1-like kinases and yeast ROM1 and ROM2 (Fig. 2 B; Ozaki et al., 1996; Nagahashi et al., 1998). Finally, both proteins contain a long coiled-coil region and a cysteine rich (C1) domain, but, interestingly, STI lacks a pleckstrin homology (PH) domain, which is thought to target proteins to the membrane or cell cortex (Rebecchi and Scarlata, 1998). *sti*^{3} encodes a truncated protein containing only part of the kinase domain, whereas *sti*^{1}, *sti*^{2}, and *sti*^{5} encode products lacking the C1 and CitroN homology domains and the last portion of the coiled-coil region. These

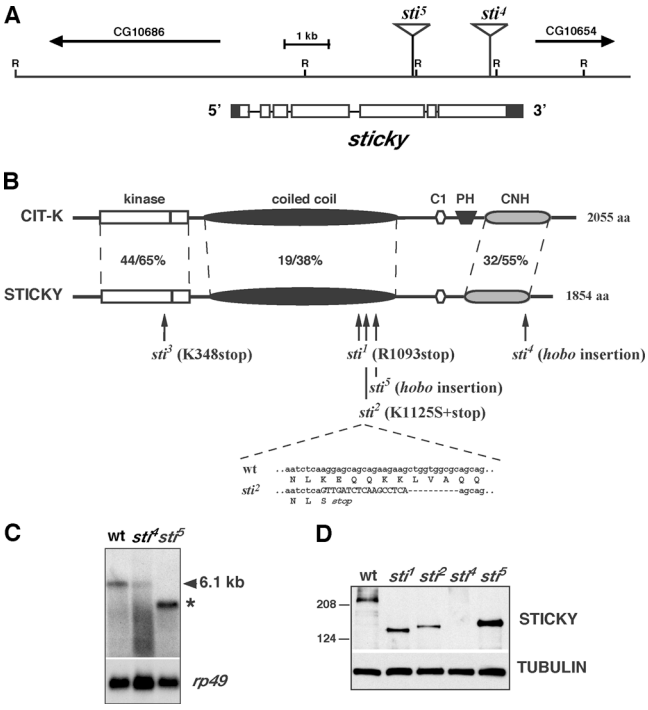

Figure 2. **Identification and molecular analysis of the *sti* gene.** (A) EcoRI restriction map of the *sti* genomic region. The two *hobo* transposable elements present in sti^4 and sti^5 and the *sti* intron/exon organization and ORF (unshaded boxes) are shown. (B) STICKY protein and its homology with Citron kinase (CIT-K). The percent of identity/similarity between corresponding domains is shown between the two proteins. Arrows indicate the mutations identified in *sti* mutants. (C) Northern blot analysis of *sti* expression in sti^4 and sti^5 mutants. 20 μg of total RNA were loaded in each lane and hybridized with *sti* and *rp49* (loading control) cDNA probes. The asterisk indicates the abnormal transcript present in sti^5 mutants. (D) Western blot analysis of STI protein expression in *sti* mutant larval brains. Proteins were extracted from w^{1118} (wt) control brains and from sti^1, sti^4, and sti^5 homozygous mutants. In the case of sti^2, proteins were extracted from brains of $sti^2/DF(3L)F10$ hemizygous larvae. Extracts were transferred to a PVDF membrane and probed with STI and tubulin (loading control) antisera.

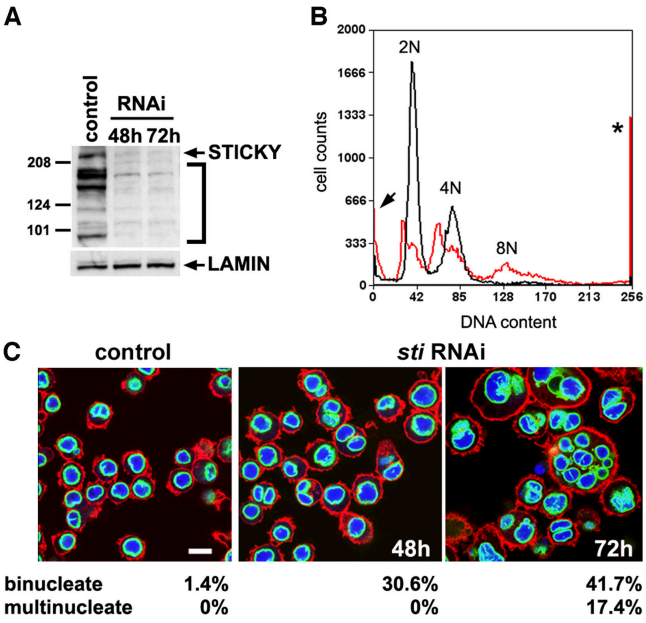

Figure 3. **RNAi-mediated silencing of *sti* in S2 cells causes cytokinesis defects.** (A) Western blot analysis of STI protein in extracts of cells treated with *sti* and GFP (control) dsRNA for 48 and 72 h. Multiple bands (indicated by the bracket) in addition to the full-length product of ~220 kD are detected and all severely reduced in STI-depleted cells. Lamin antibody was used as loading control. (B) FACS® profiles of cells treated with GFP (control, black) and *sti* (red) dsRNA for 72 h. The arrow indicates potential apoptotic cells (low or no DNA content), whereas the asterisk marks highly polyploid cells. (C) Confocal images of GFP (control) and *sti* dsRNA treated cells stained to detect F-actin (red), lamin (green), and DNA (blue). The percentage of bi- and multinucleate cells is shown at the bottom, >1,000 cells were counted for each sample. Bar, 10 μm.

molecular data are in strong agreement with the genetic results presented earlier. Finally, it is noteworthy that although sti^5 is a much weaker allele than sti^2, the difference in length between the two mutated proteins is only 53 aa. This indicates that the region lying between residues 1125 and 1178 is important for STI activity.

RNAi-mediated silencing of *sti* leads to the formation of multinucleate cells

To further show that *sti* is essential for cytokinesis, we used RNAi to inactivate its function(s) in *Drosophila* Schneider 2 (S2) cells. As shown in Fig. 3 A, most of the STI protein was depleted after incubation of S2 cells with *sti* dsRNA for 48 or 72 h. Several bands were detected in S2 cell extracts and all were specifically depleted after RNAi treatment. We believe that these bands correspond to degradation products in S2 cells, as we never detected multiple protein or mRNA isoforms in our previous experiments (Fig. 2, C and D). Moreover, immunolocalization experiments (see below; Fig. 5) also suggested that STI protein is likely to be degraded at the end of cell division.

Flow cytometric analysis (FACS®) revealed that depletion of STI causes an increase of polyploid (8N or more) together with aneuploid cells (Fig. 3 B). In addition, the number of putative apoptotic cells was higher in STI-treated cells respective to the controls, suggesting that the increase in polyploidy can, at some point, trigger cell death (Fig. 3 B, arrow). Immunostaining experiments confirmed that polyploidy in STI-deficient cells results from defects in cytokinesis (Fig. 3 C). The percentage of bi/multinucleate cells increased after incubating for 48 and 72 h with *sti* dsRNA by ~21 and 42 times, respectively. The nuclei present in binucleate cells following *sti* RNAi after 48 h were of similar size suggesting that inactivation of *sti* in S2 cells produces a block in cytokinesis (Fig. 3 C). Very large cells containing up to 10–12 nuclei could be observed in cultures treated for 72 h (Fig. 3 C), indicative of failure of cytokinesis in multiple cycles.

STI-deficient cells display asymmetric furrowing and abnormal blebbing

To confirm directly a failure of cytokinesis after *sti* RNAi, we observed cells by time-lapse microscopy. In control, GFP dsRNA transfected cells ($n = 6$), the cytoplasm began to

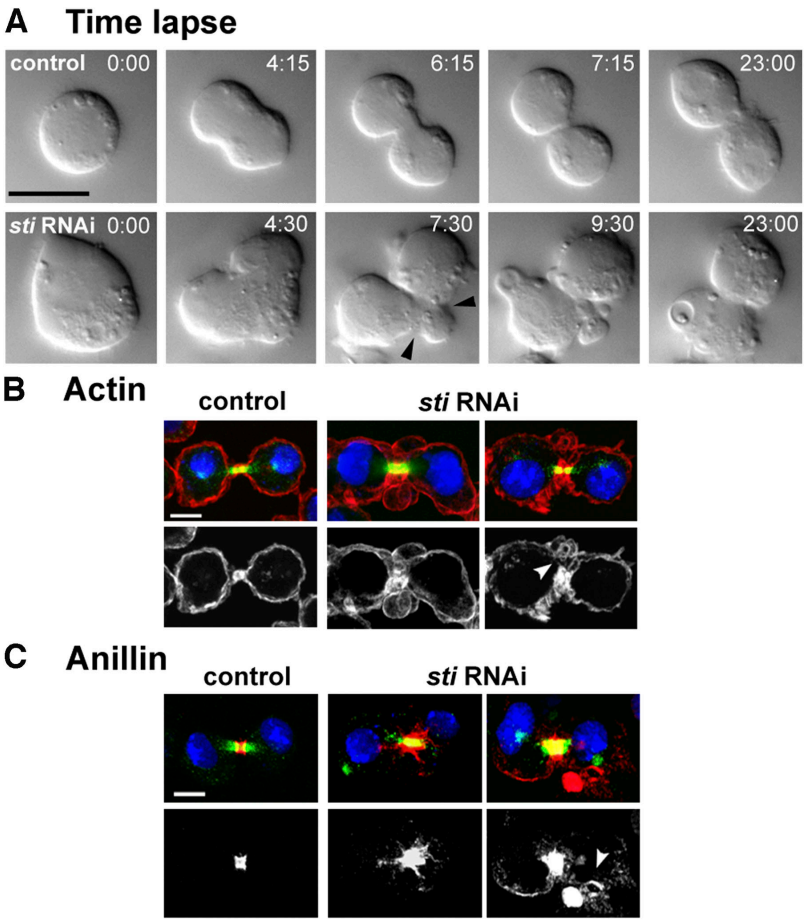

Figure 4. **Morphological analysis of cytokinesis defects in STI-depleted cells.** (A) Selected images from time-lapse recordings of S2 cells after incubation with GFP (control) or *sti* dsRNA (*sti* RNAi) for 72 h. The *sti* RNAi cell appears larger than the control, but chromosome complement and spindle size/morphology indicate that this cell is not polyploid. Time is in min/s after anaphase onset (0:00 time point). The arrowheads mark an ectopic contractile ring. Bar, 10 μm. (B) S2 cells were incubated with either GFP (control) or *sti* dsRNA for 48 or 72 h and then fixed and stained to reveal F-actin (red), microtubules (green), and DNA (blue). The bottom panel shows the monochromic channel for F-actin. The arrowhead indicates a gap in the actin ring structure. Bar, 5 μm. (C) S2 cells were incubated with either GFP (control) or *sti* dsRNA for 48 or 72 h and then fixed and stained to reveal Anillin (red), microtubules (green) and DNA (blue). The bottom panel shows the monochromic channel for Anillin. The arrowhead marks an ectopic contractile ring. Bar, 5 μm.

constrict symmetrically at the spindle equator within 5 ± 1 min of anaphase onset (Fig. 4 A, top; 4:15 time point; Video 1, available at http://www.jcb.org/cgi/content/full/jcb.200402157/DC1). Furrow ingression was rapid and a midbody formed shortly thereafter (Fig. 4 A, 7:15), linking the two daughter cells together for the duration of filming (Fig. 4 A, 23:00). In STI-depleted cells (n = 7), chromosome congression, alignment and segregation appeared normal (Fig. 4 A, bottom and not depicted; Videos 2 and 3, available at http://www.jcb.org/cgi/content/full/jcb.200402157/DC1) and the timing of furrow initiation was also unaffected (4 ± 1 min). However, in about half of these cells (4 out of 7) a "unilateral furrow" was initiated (Fig. 4 A, 4:30) and advanced across the cytoplasm before joining with one or two less robust furrows (Fig. 4 A, 7:30, arrowheads; Videos 2 and 3). This asymmetric furrowing was accompanied by a series of highly dynamic equatorial protrusions that could culminate in the formation of ectopic contractile rings (Fig. 4 A, 9:30; Fig. 4 C, arrowhead; Videos 2 and 3). Although some blebbing also occurred in control cells, this was usually confined to nonequatorial locations and was much less dramatic than observed in STI-depleted cells. Abnormal blebbing was only observed during cytokinesis in *sti* RNAi cells (Fig. 3 C; not depicted). Unfortunately, we were unable to follow cells for longer than 35 min after anaphase onset and this prevented our direct observation of cell abscission in both control and *sti* RNAi treated cells. Nonetheless, the experiments shown in Fig. 3 clearly reveal that *sti*-deficient cells become multinucleate. Therefore, we propose that these cells are unable to complete cytokinesis as a consequence of the altered dynamics of events occurring during furrow ingression.

To understand these aberrant phenotypes, we first examined the localization of several central spindle and contractile ring components after *sti* RNAi. The morphology of the central spindle and the localization of factors essential for its formation, including the Aurora B kinase, PAV-KLP, and RacGAP50C, appeared completely normal in STI-deficient cells (Fig. 4, B and C; Fig. 5 A; not depicted; Adams et al., 1998; Giet and Glover, 2001; Somers and Saint, 2003). In contrast, contractile ring components such as F-actin, Anillin, and the septin Peanut localized normally at cleavage furrow formation (Fig. S1, available at http://www.jcb.org/cgi/content/full/jcb.200402157/DC1), but displayed aberrant accumulation and distribution in late telophase (Fig. 4, B and C; not depicted; Neufeld and Rubin, 1994; Field and Alberts, 1995). F-actin appeared very disorganized in *sti* RNAi cells and less compact than in control cells (compare Fig. 4 B with Fig. 5 B). Actin also appeared to diffuse inside the equatorial membrane protrusions (Fig. 4 B, middle) and *sti*-deficient cells showed gaps in the actin ring structure that may reflect unilateral furrowing (Fig. 4 B, right, arrowhead). Anillin, an actin-binding protein that has been postulated to interact with the membrane and the actomyosin ring (Giansanti et al., 1999; Somma et al., 2002), also accumulated abnormally in *sti* RNAi late telophases (Fig. 4 C). In some se-

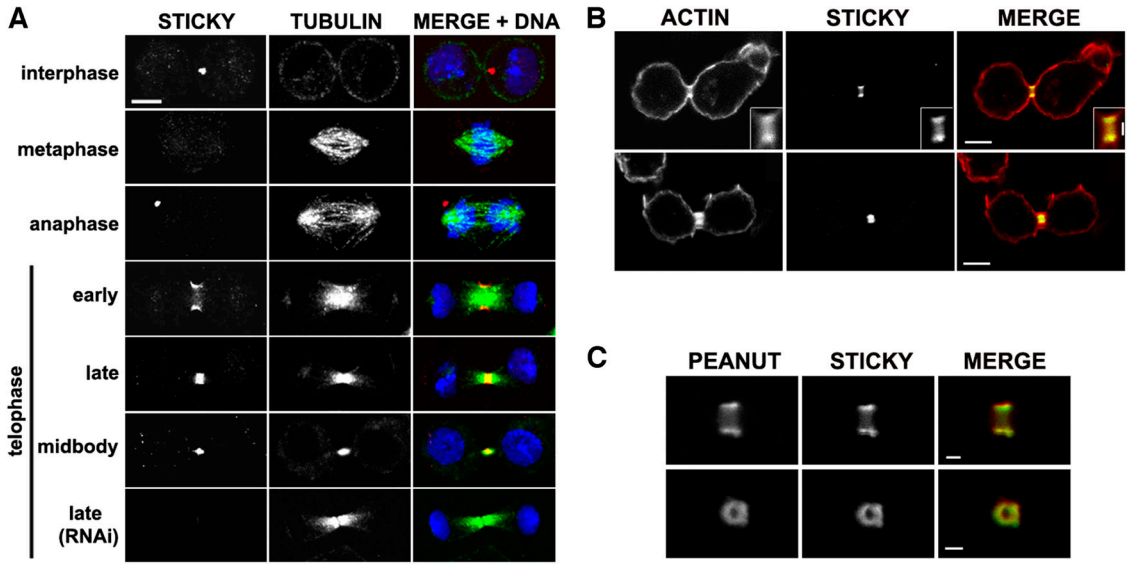

Figure 5. **Subcellular localization of STI protein.** (A) *Drosophila* S2 cells were fixed and stained to reveal STI (red), tubulin (green), and DNA (blue). The monochromic channels relative to STI (left) and tubulin (middle) are also shown. The bottom panel shows a *sti* RNAi-depleted cell at late telophase. Bar, 5 μm. (B) Cells at late telophase (top) and midbody (bottom) stage were fixed and stained to detect F-actin (red) and STI (green). Monochromic channels showing F-actin (left) and STI (middle) are also shown. The inset shows a higher magnification of the contractile ring. Bar, 5 μm; inset, 1 μm. (C) Two different sections of contractile rings stained to reveal STI (green) and the septin-like protein peanut (red). Monochromic channels showing peanut (left) and STI (middle) are also shown. Bar, 1 μm.

vere situations, Anillin also marked the formation of ectopic contractile rings (Fig. 4 C, arrowhead). Finally, it should be noted that, although depletion of STI altered both the morphology and organization of the contractile ring, the furrow was still able to constrict completely to form, at least transiently, a midbody-like structure (Fig. 4, A–C; Fig. 5 A; Videos 2 and 3). This observation indicates that actomyosin filaments can contract normally when STI is depleted, in contrast with what has been proposed for its mammalian counterpart, CIT-K (Madaule et al., 2000).

STICKY localizes to the cleavage furrow beneath the actomyosin ring

In interphase S2 cells, our affinity-purified STI antibody detected punctate signals in the cytoplasm and in the nucleus. In addition, some cells showed strong dot-like STI staining that we believe to be midbody remnants (Fig. 5 A). A similar staining pattern was observed in meta- and anaphase, but as cells enter telophase, STI localized to the ingressing cleavage furrow and formed a ring around the midzone microtubules to concentrate into the midbody at the end of telophase (Fig. 5 A). In cells treated with *sti* dsRNA, the signal detected throughout the cell cycle was either absent or extremely weak (Fig. 5 A, bottom; not depicted). Co-staining to detect F-actin (Fig. 5 B) revealed STI localized underneath the actomyosin ring (Fig. 5 B, top). This localization became particularly evident in cells at the midbody stage (Fig. 5 B, bottom). In addition, STI also appeared to colocalize with the septin peanut (Fig. 5 C; Neufeld and Rubin, 1994). These results suggest that STI might be a component of the contractile ring, but probably does not interact directly with the cell membrane. This is consistent with STI not having a PH domain like its mammalian counterpart CIT-K.

sti interacts genetically with *Rho* and *Rac*

Several lines of evidence have indicated that RhoA activates CIT-K in vitro (Madaule et al., 1995; Di Cunto et al., 1998; Eda et al., 2001). To investigate STI regulation by the family of small Rho GTPases in vivo, we used a genetic approach. To this end, we created transgenic fly lines in which *sti* functions can be partially silenced by RNAi in specific tissues using the GAL4/UAS system (Brand and Perrimon, 1993). The expression of *sti* dsRNA in the developing eye tissue using the *ey-GAL4* driver and two copies of a *SymUAS-sti* reporter (Bonini et al., 1997; Giordano et al., 2002) led to the formation of multinucleate cells (Fig. 6 B). As a likely consequence, the emerging adults had eyes considerably smaller than wild type and composed of large and disorganized ommatidia (Fig. 6, C and D). This "rough" eye phenotype was enhanced by the presence in the genome of a strong *sti* mutation, sti^3, consistent with the effect being caused by inactivation of the *sti* gene (Fig. 6 E). The *sti* eye phenotype was also significantly enhanced by null mutations in the single *Drosophila* RhoA homologue, *Rho1* (Fig. 6 F; Strutt et al., 1997). Interestingly, a chromosome mutated in the three *Drosophila* Rac genes, *Rac1*, *Rac2*, and *Mtl* (*triRac*) (Hakeda-Suzuki et al., 2002; Ng et al., 2002), was able to dominantly suppress the *sti* phenotype almost completely, reverting the eye to wild-type size and appearance (Fig. 6 G). A very similar suppression was obtained with mutations only in the *Rac1* and *Rac2* genes (unpublished data).

Yamashiro et al. (2003) have recently shown that CIT-K is able to phosphorylate the MRLC at both serine-19 and threonine-18 residues in vitro. To investigate if the MRLC encoded by the *spaghetti squash* (*sqh*) gene is a STI target in vivo, we used a transgenic fly stock carrying a mutated form of the *sqh* gene, sqh^{E20E21}, in which both Ser-21 and Thr-20

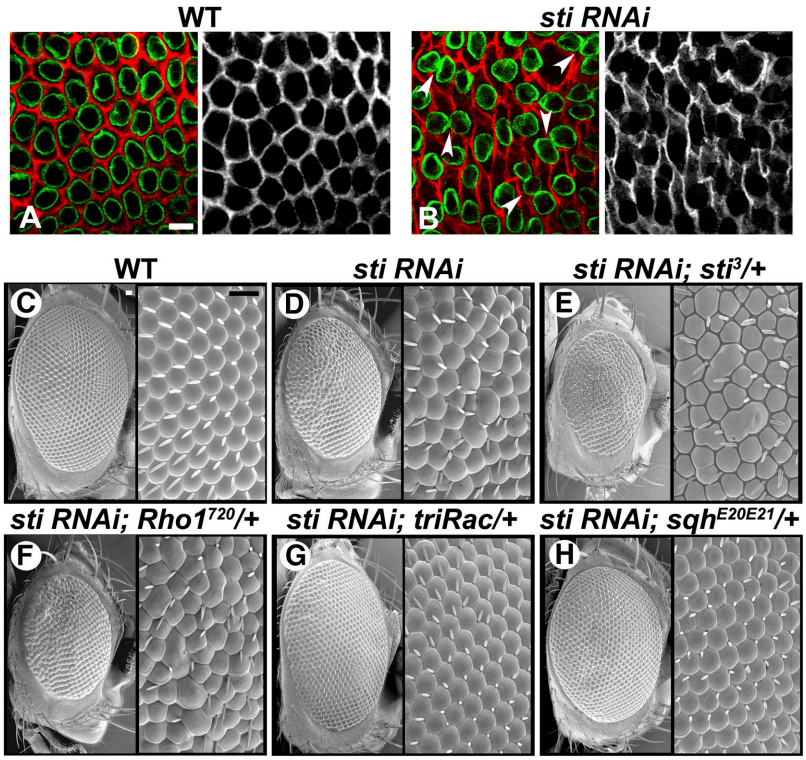

Figure 6. ***sti* interacts genetically with *Rho* and *Rac* genes.** WT (A) and *sti* RNAi (B) imaginal discs were fixed and stained to reveal lamin (green) to mark the nuclear envelope and the membrane-skeleton protein Coracle (red) to mark cell boundaries. Monochromic channels showing only Coracle staining are shown on the right. Arrowheads indicate examples in which the membranes of different nuclei are in contact. Bar, 5 μm. Scanning electron micrographs of wild-type (C, WT), *ey-GAL4>SymUAS-sti* (D, *sti RNAi*), *ey-GAL4>SymUAS-sti; sti*^{3}/+ (E, *sti RNAi; sti*^{3}/+), *ey-GAL4>SymUAS-sti; Rho1*^{720}/+ (F, *sti RNAi; Rho1*^{720}/+), *ey-GAL4>SymUAS-sti; Rac1*^{J11}, *Rac2*$^{\Delta}$, *Mtl*$^{\Delta}$/+ (G, *sti RNAi; triRac/+*), *ey-GAL4>SymUAS-sti; sqh*^{E20E21}/+ (H, *sti RNAi; sqh*^{E20E21}/+) adult fly eyes. Expression of sti dsRNA in the developing eye reduces its size and alters the organization and dimension of the ommatidia (D). A single copy of the *sti*^{3} mutation enhances this phenotype (E). A null mutation in the *Drosophila* RhoA homologue, *Rho1*^{720}, acts as a dominant enhancer (F). A chromosome containing mutations in the three *Drosophila Rac* genes, *Rac1*^{J11}, *Rac2*$^{\Delta}$, *Mtl*$^{\Delta}$, dominantly suppresses the sti RNAi phenotype (G). A transgene containing a phosphomimic version of the *sqh* gene, *sqh*^{E20E21}, acts as a dominant suppressor (H). Bar, 20 μm.

(equivalent to vertebrate Ser-19 and Thr-18) have been replaced by the phosphomimic residue glutamic acid (E) (Jordan and Karess, 1997). This mutated protein behaves in vivo as a phosphorylated version of SQH, inasmuch as it is able to rescue the lethality associated with strong mutations in the *Drosophila* ROK (*rok*) gene (Winter et al., 2001). As shown in Fig. 6 H, a single copy of the *sqh*^{E20E21} transgene was able to suppress considerably the *sti* rough eye phenotype, suggesting the possibility that SQH can be phosphorylated by STI in vivo.

RacGAP50C phenotypes are enhanced by *Rho* and suppressed by *Rac*

Our genetic evidence that *Rac* genes dominantly suppress the *sti* RNAi phenotype suggests the possibility that Rac GTPases may play an inhibitory role during cytokinesis (Fig. 6). Loss of function studies in *Drosophila* and other animals have not previously implicated Rac in cytokinesis (Lundquist et al., 2001; Gu and Williams, 2002; Hakeda-Suzuki et al., 2002; Ng et al., 2002). These studies, however, could only indicate that Rac GTPases are not essential for this process, but do not rule out the possibility that the activity of these GTPases needs to be down-regulated during cytokinesis. Identification of a Rac repressor that is essential for cytokinesis would provide further evidence for such an inhibitory role. The *Drosophila* RacGAP50C has been implicated in cytokinesis, but its target GTPase has not been clearly identified yet (Somers and Saint, 2003). Thus, we investigated whether RacGAP50C could inhibit Rac activity in vivo. Expression of *RacGAP50C* dsRNA in developing

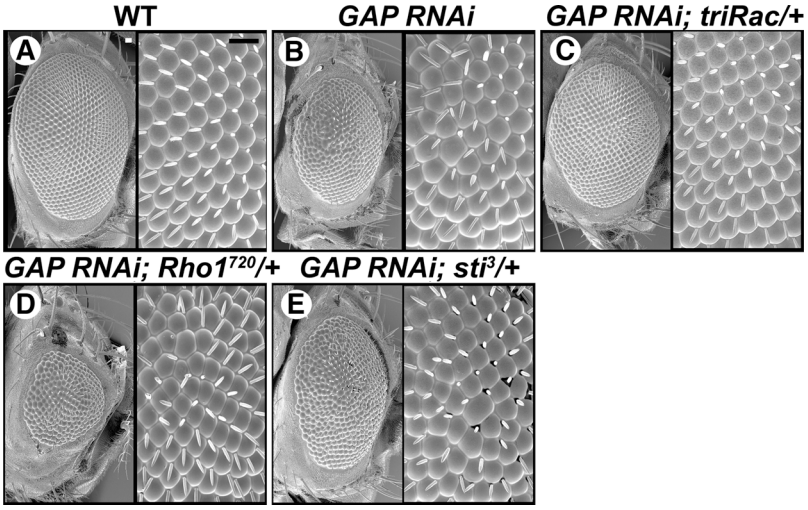

Figure 7. **RaGAP50C inhibits Rac and promotes Rho activity.** Scanning electron micrographs of wild-type (A; WT), *ey-GAL4>UAS-RacGAP50C.dsRNA* (B, *GAP RNAi*), *ey-GAL4>UAS-RacGAP50C.dsRNA; Rac1*^{J11}, *Rac2*$^{\Delta}$, *Mtl*$^{\Delta}$/+ (C, *GAP RNAi; triRac/+*), *ey-GAL4>UAS-RacGAP50C.dsRNA; Rho1*^{720}/+, (D, *GAP RNAi; Rho1*^{720}/+), *ey-GAL4>UAS-RacGAP50C.dsRNA; sti*^{3}/+ (E, *GAP RNAi; sti*^{3}/+) adult fly eyes. Expression of RacGAP50C dsRNA in the developing eye reduces its size and alters the organization and dimension of the ommatidia (B). A chromosome containing null or strong mutations in the three *Drosophila Rac* genes, *Rac1*^{J11}, *Rac2*$^{\Delta}$, *Mtl*$^{\Delta}$, dominantly suppresses this phenotype (C). A null mutation in the *Drosophila* RhoA homologue, *Rho1*^{720}, acts as a dominant enhancer (D). (E). The *sti*^{3} mutation does not modify the phenotype. Bar, 20 μm.

imaginal tissues led to the formation of multinucleate cells and its RNAi-mediated silencing during eye development resulted in a significant reduction of the adult eye (Fig. 7 B; Billuart et al., 2001; Somers and Saint, 2003). These eyes contained large and disorganized ommatidia, very similar to *sti* RNAi mutants (compare Fig. 6 B with Fig. 7 B). A chromosome carrying mutations in all three Rac genes, (*triRac*), dominantly suppressed this phenotype (Fig. 7 C; Hakeda-Suzuki et al., 2002; Ng et al., 2002), whereas *Rho* mutations acted as strong enhancers (Fig. 7 D; Strutt et al., 1997). These observations are consistent with RacGAP50C inhibiting Rac and promoting Rho activity. Finally, the strongest *sti* mutation available, sti^3, failed to significantly enhance or suppress the *RacGAP50C* eye phenotype (Fig. 7 E). This result suggests that *sti* does not function in a pathway between *Rho* and *RacGAP50C* as discussed below.

Discussion

sti encodes the *Drosophila* orthologue of CIT-K

Database searches identified STI as the closest *Drosophila* relative of the mammalian CIT-K, and other findings strongly suggest that it is its functional homologue. The two proteins show corresponding subcellular localization in both insect and mammalian cells. They appear to form protein aggregates during interphase and the early stages of mitosis and then localize to the cleavage furrow during telophase and to the midbody at the end of cell division (Fig. 5; Eda et al., 2001). Our genetic evidence indicate that STI kinase is positively regulated by Rho consistent with in vitro and in vivo studies with mammalian CIT-K (Fig. 6; Di Cunto et al., 1998; Madaule et al., 1995, 1998). It is important to note, however, three major differences between STI and CIT-K. First, CIT-K is only required for cytokinesis in testes and specific neuronal populations in mice (Di Cunto et al., 2000, 2002), whereas STI is essential for cell division in all *Drosophila* proliferating tissues we have examined, including all the imaginal discs and the brain. Second, multiple CIT-K isoforms have been described in mouse and HeLa cells (Di Cunto et al., 1998; Madaule et al., 2000), whereas we have observed only a single *sti* transcript in *Drosophila* larvae and only one protein in brain extracts (Fig. 2). Third, STI does not contain a PH domain like CIT-K, and consistent with this observation STI protein does not appear to localize to the cell membrane (Fig. 5). Altogether these data suggest that STI and CIT-K originate from the same ancestral protein, but the mammalian product may have lost some of its original functions and acquired new ones during evolution.

sti controls the organization and structure of the contractile ring

We show in *sti*-depleted cells the recruitment of central spindle and contractile ring components is normal during telophase (Fig. S1; not depicted). However, these cells display uncoordinated furrow constriction and abnormal blebbing (Fig. 4 A; Videos 2 and 3). These phenotypes are accompanied by a less compact ring structure, unusual F-actin formations and abnormal accumulation of the contractile ring component Anillin (Fig. 4, B and C). In some situations, *sti* RNAi cells also exhibit supernumerary contractile rings (Fig. 4 C; Videos 2 and 3). These defects are consistent with problems in controlling the organization and/or structure of the contractile ring. The presence of unusual F-actin formations also suggests that STI-depleted cells are unable to control actin depolymerization and behavior during cytokinesis. Interestingly, very similar phenotypes have been observed in Anillin-depleted cells, suggesting that one *sti* function might be to regulate the interaction between F-actin and Anillin during cytokinesis (Somma et al., 2002).

The identification of STI targets will be crucial to fully comprehend how this kinase regulates the organization of the contractile ring during cytokinesis. The genetic experiment shown in Fig. 6 indicates that one potential STI target is the MRLC encoded by the *sqh* gene, as a phosphomimic version of this protein rescues the *sti* rough eye phenotype. However, MRLC phosphorylation by STI does not seem to regulate actomyosin ring contractility but rather its organization and/or structure (Fig. 4). How can the MRLC phosphorylation status affect contractile ring structure? A recent study has indicated that CIT-K induces diphosphorylation, rather than monophosphorylation, of the MRLC (Yamashiro et al., 2003). These authors also observed that diphosporylated MRLC shows more constrained localization at the cleavage furrow than the monophosphorylated form. These results, together with previous observations that MRLC diphosphorylation can affect filament assembly (Ikebe and Hartshorne, 1985), led the authors to propose that diphosphorylated MRLC may play a role in cross-linking of actin filaments rather that stimulation of motor activity. In conclusion, these data suggest that diphosphorylation of the MRLC by STI/CIT-K induces a conformational change of the actomyosin filament structure that is essential for proper assembly of the contractile ring.

Antagonism between Rho and Rac GTPases regulates cytokinesis

As discussed above, in vitro studies have indicated that RhoA promotes CIT-K enzymatic activity (Di Cunto et al., 1998). Consistently, our in vivo genetic data show that mutations in *Rho1*, the *Drosophila* RhoA homologue, dominantly enhance the *sti* RNAi phenotype (Fig. 6). Intriguingly, our experiments also show that *Rac* mutations dominantly suppress the *sti* and *RacGAP50C* RNAi phenotypes (Figs. 6 and 7), suggesting that Rac GTPases need to be down-regulated during cytokinesis. Previous studies using *Rac* loss of function mutants probably failed to reveal such an inhibitory role because the absence of negative regulators would not impair cytokinesis (Hakeda-Suzuki et al., 2002; Ng et al., 2002). Other recent studies also suggest that Rac inhibition might be important for cytokinesis. First, fluorescence resonance energy transfer analysis has demonstrated that Rac activity is strongly reduced at the cleavage furrow during cytokinesis (Yoshizaki et al., 2003). Second, inducible expression of a constitutive active form of Rac in PAE cells induces the formation of multinucleate cells (Muris et al., 2002). Cross-talk among members of different GTPase subfamilies is not unusual and antagonism between

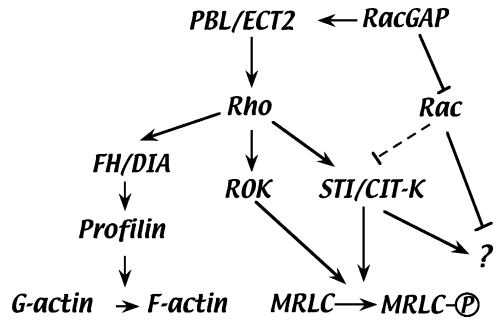

Figure 8. **A model illustrating the antagonism between Rho and Rac GTPases during cytokinesis.** The details are explained in the text. The dotted line indicates that the interaction between Rac and STICKY need not to be direct. The question mark indicates other putative STI targets that have yet to be identified.

Rho and Rac has been described in other cellular processes (Burridge and Wennerberg, 2004). Thus, a similar antagonism may also regulate the dynamics of the contractile ring. Why would Rac GTPases need to be repressed during cytokinesis? Several data indicate that the success of cytokinesis depends not only on the contraction of the actomyosin-based machinery (activated by Rho), but also on reduced stiffness at the cortex (Robinson and Spudich, 2000). Thus, one possible explanation of our results is that Rac inhibition may diminish cortical stiffness and help furrow ingression.

Genetic interaction experiments indicate that genes function in the same biological process, but not necessarily in the same pathway. However, because in our experiments the suppression of *sti* and *RacGAP50C* RNAi phenotypes by *Rac* mutations is dominant, it is conceivable that they act in the same, rather than in a parallel, pathway. In this scenario, RacGAP50C might be expected to inhibit Rac through a direct protein-protein interaction mechanism. On the other hand, two opposite explanations exist for the relationship between *sti* and *Rac*: either Rac represses STI or STI inhibits Rac. Under the second hypothesis, however, Rac inhibition by STI should be indirect, as GTPase activity is generally regulated by cofactors (i.e., GEFs and GAPs) and not by phosphorylation. Because the experiments shown in Fig. 7 indicate that RacGAP50C represses Rac activity, the second hypothesis would implicate a linear pathway in which Rho activates STI, which in turn activates RacGAP50C, which ultimately inhibits Rac GTPases. This is in contrast with our findings that *sti* does not enhance the *RacGAP50C* RNAi phenotype whereas *Rho1* does, suggesting that these factors do not function in a simple linear pathway. For these reasons we favor the alternative model depicted in Fig. 8. In this model, RacGAP50C plays a key role by inhibiting Rac and promoting Rho activity, probably through its interaction with the PBL/ECT2 GEF as suggested by the results of Somers and Saint (2003). The two GTPases then antagonistically regulate STI activity. This regulation could be direct, as both GTPases bind CIT-K in vitro (Madaule et al., 1995), but our genetic data do not exclude the possibility that Rac regulates STI through one or more intermediates. We also cannot discount the hypothesis that Rac inhibits the function of proteins that are activated by STI (Fig. 8). Further functional and structural analysis of STI will be required to understand the molecular mechanisms that control the activity of this kinase. One implication of the model shown in Fig. 8 is that even slight variations in the equilibrium of the factors could easily alter the dynamics of contractile ring components during cytokinesis. For example, RacGAP50C activation could promote RhoA activity and consequently actomyosin filament assembly and contraction (Fig. 8). Conversely, RacGAP50C inhibition would both down-regulate Rho and activate Rac to repress STI thereby promoting filament disassembly.

Materials and methods

Fly stocks, genetics, and cytology

The Or-R and w^{1118} stocks were used as wild type. The sti^{1} allele has been described previously (Gatti and Baker, 1989). The sti^{2} and sti^{3} alleles were generated in a standard chemical mutagenesis using ethylnitrosurea. The deficiencies *Df(3L)F10* and *Df(3L)E44* are described in Flybase (http://flybase.bio.indiana.edu/). The *Rho1* alleles are described in Strutt et al. (1997). The sqh^{E20E21} stock was provided by R. Karess (Centre de Génétique Moléculaire, Gif-sur-Yvette, France) and is described in Jordan and Karess (1997). The *Rac* mutants (Hakeda-Suzuki et al., 2002; Ng et al., 2002), and the *ey-GAL4* (Bonini et al., 1997) and *UAS-RacGAP50C.dsRNA* (Billuart et al., 2001) transgenic fly stocks were obtained from the Bloomington Stock Center. *sti* was initially mapped between *h* and *th* by meiotic mapping and subsequently to the polytene region 69D2-3 in a small area uncovered by two overlapping deficiencies, *Df(3L)F10* (breakpoints 69A1; 69D2-3) and *Df(3L)E44* (breakpoints 69D2; 69E3-5). Lethal phase analysis of *sti* mutants was performed as described previously (D'Avino and Thummel, 1998). Preparations of neuroblast mitotic chromosomes are described in Gonzalez and Glover (1993).

Cloning and analysis of *sti*

DNA extraction and Southern blot analysis were performed as described in D'Avino and Thummel (1998). To identify potential RFLPs in sti^{4} and sti^{5} mutants, genomic DNA was probed with PCR fragments generated at 2–3-kb intervals in the genomic regions flanking both sides of the *vihar* gene. Four different cDNAs correspondent to the CG10522 gene, LD04032, LD18858, LD09587, and RE26327, were sequenced on both strands. The longest cDNA, RE26327, appeared to be full length. Intron/exon organization was obtained by comparing the sequence of the *sti* cDNAs and the genomic sequence available from the BDGP (http://www.fruitfly.org/). To identify the molecular lesions of *sti* mutants, the entire *sti* genomic region (~7 kb) was PCR amplified from *sti* mutant genomic DNAs using the Expand Long Template PCR System (Roche). The PCR products were then cloned into pGEM-T (Promega) and sequenced on both strands. Two distinct PCR products were sequenced for each *sti* allele. For the Northern blot described in Fig. 2 D, total RNA was extracted from w^{1118} and *sti* mutant larvae, fractionated by formaldehyde agarose gel electrophoresis, and blotted as described previously (D'Avino et al., 1995).

Generation of STI antibodies and Western blot analysis

STI antibodies were generated in rabbits against a fragment of the STI protein (amino acids 531–742) fused to a carboxy-terminal 6XHis tag. Two different rabbits were injected and STI specific antibodies were affinity purified using the STI-6His-tagged recombinant protein linked to CNBr-activated Sepharose 4B beads (Amersham Biosciences). The affinity-purified antibodies were used at a final concentration of 1:800 for cell immunostainings and 1:3,000 for Western blot analysis. For Western blot analysis, larval brains, or S2 cells were homogenized in Laemmli buffer, subjected to three cycles of freezing/boiling, and centrifuged for 15′ at 4°C to recover the supernatant. Protein extracts were separated by 8% SDS-PAGE and transferred on a PVDF membrane (Millipore).

Cell culture, FACS® analysis, RNAi, and microscopy

Drosophila Schneider2 (S2) cells were grown at 25°C in Schneider's medium supplemented with 10% FCS (Sigma-Aldrich). For FACS® analysis, cells were harvested, washed with PBS, and fixed in 90% ice-cold ethanol. Fixed cells were then washed in PBS and incubated with 40 μg/ml RNase A and 1 μg/ml propidium iodide at 37°C for 30 min. Cells were analyzed using FACScan™ equipment (BD Biosciences). For RNAi experiments, ~600-bp PCR fragments of the *sti* and GFP (control) coding regions con-

taining tails coding for the T7 promoter were transcribed in vitro using the RiboMAX System (Promega). 10 μg of dsRNA were used to transfect 2 × 10^6 cells in a 35-mm Petri dish using TransFast Reagent (Promega). For immunolocalization experiments, cells were fixed and stained as described by Giet and Glover (2001). Eye imaginal discs were dissected by hand, fixed and stained as described previously (Brakefield et al., 1996). Images were acquired using a 1024 confocal (Bio-Rad Laboratories). The following antibodies and working dilutions were used: rat antitubulin, 1:40 (clone YL1/2; Sigma-Aldrich); rabbit anti-Anillin, 1:1,500 (provided by C. Field, Harvard Medical School, Boston, MA; Field and Alberts, 1995); rabbit anti–Aurora B, 1:200 (Giet and Glover, 2001); rabbit anti-Pavarotti, 1:200 (Minestrini et al., 2002); mouse anti-peanut, 1:4 (Neufeld and Rubin, 1994); rat anti-RacGap50C, 1:400 (a gift from R. Saint, University of Adelaide, Adelaide, Australia); T47 mouse anti-lamin, 1:40 (Paddy et al., 1990); and guinea pig anti-coracle 1:1,200 (Fehon et al., 1994). Alexa-conjugated secondary antibodies and rhodamine-phalloidin were purchased from Molecular Probes. For time-lapse microscopy, S2 cells were grown on clean No. 1 1/2 thickness coverslips. 3 d after transfection, the coverslips were mounted on a 65-μl gene frame (ABgene). Time-lapse microscopy was performed on a Axiovert 200 microscope (Carl Zeiss MicroImaging, Inc.) outfitted with differential interference contrast optics using a 100× (N.A. 1.4) objective lens. Cells were illuminated with filtered, 546 nm of light. Shuttering and image acquisition were controlled with Metamorph (Universal Imaging Corp). Images were captured at 15-s intervals using a Coolsnap HQ (Photometrics) camera with a 2 × 2 bin. Cells were maintained at 25 ± 1°C during filming.

Generation of *sti* RNAi transgenic flies and genetic interaction experiments

A 2.5-kb EcoRI fragment containing most of the exons 4 and 5 and relative intron (Fig. 2) was cloned in the pSym-UAST vector (provided by E. Giordano, University of Naples, Naples, Italy; Giordano et al., 2002) and injected in w^{1118} embryos using standard protocols to generate *Sym-UAS-sti* transgenic flies. Two copies of the *Sym-UAS-sti* transgene interfered with normal eye development (Fig. 6). For the experiments shown in Fig. 6, we created a stock containing four copies of the *Sym-UAS-sti* transgene and one copy of the *ey-GAL4* driver, *y w Sym-UAS-sti*^{33X}; eye-GAL4/CyO; Sym-UAS-sti^{49III}. Virgin females were collected from this stock and crossed to males heterozygous for *sti*, *Rho1, pbl*, *sqh*^{E20E21}, double (*Rac1*^{J11} + *Rac2*$^{\Delta}$) or triple *Rac* (*Rac1*^{J11} + *Rac2* + *Mtl*$^{\Delta}$) mutations and a dominantly marked balancer chromosome (*CyO* y^{+} or *TM6B, Tb*). Typically, five virgin females were crossed to five males in a 2-cm diam vial at 25°C. These adults were then transferred every 24 h into a fresh vial and the embryos incubated at 29°C until eclosion. For *RacGAP50C* experiments, the *UAS-RacGAP50C.dsRNA* insert as described in Billuart et al. (2001) was recombined onto the *ey-GAL4* chromosome (Bonini et al., 1997). *y w*; *ey-GAL4, UAS-RacGAP50C.dsRNA/CyO* virgin females were crossed to males heterozygous for the appropriate mutation(s) as described above and the progeny was incubated at 25°C until eclosion.

Online supplemental material

Video 1 shows cytokinesis in a S2 cell transfected with GFP dsRNA (control) for 72 h. Videos 2 and 3 show cytokinesis in two different cells treated with *sti* dsRNA for 72 h. All sequences were captured at 15-s intervals; playback rates are 6 frames/s. Fig. S1 shows Actin (A) and Anillin (B) localization in early telophases of control (GFP-treated) and *sti* RNAi cells. Microtubules are shown in green and DNA in blue in the merged panels. The bottom panels show the monochromic channels for Actin and Anillin. Bar, 5 μm. Online supplemental material is available at http://www.jcb.org/cgi/content/full/jcb.200402157/DC1.

We are very grateful to A.T. Carpenter for her help with the genetic mapping of *sti* and for the *sti*^{2} and *sti*^{3} alleles, and to G. Kingshott for injections. We also thank R. Karess, C. Field, E. Giordano, R. Saint, and the Bloomington stock center for reagents.

This work was supported by grants from the Cancer Research-UK, UK Medical Research Council, and European Union to D.M. Glover; and by an MRC Cambridge *Drosophila* Co-operative Group grant.

Submitted: 29 February 2004
Accepted: 24 May 2004

References

Adams, R.R., A.A. Tavares, A. Salzberg, H.J. Bellen, and D.M. Glover. 1998. *Pavarotti* encodes a kinesin-like protein required to organize the central spindle and contractile ring for cytokinesis. *Genes Dev.* 12:1483–1494.

Amano, M., M. Ito, K. Kimura, Y. Fukata, K. Chihara, T. Nakano, Y. Matsuura, and K. Kaibuchi. 1996. Phosphorylation and activation of myosin by Rho-associated kinase (Rho-kinase). *J. Biol. Chem.* 271:20246–20249.

Billuart, P., C.G. Winter, A. Maresh, X. Zhao, and L. Luo. 2001. Regulating axon branch stability: the role of p190 RhoGAP in repressing a retraction signaling pathway. *Cell.* 107:195–207.

Bonini, N.M., Q.T. Bui, G.L. Gray-Board, and J.M. Warrick. 1997. The *Drosophila eyes absent* gene directs ectopic eye formation in a pathway conserved between flies and vertebrates. *Development.* 124:4819–4826.

Brakefield, P.M., J. Gates, D. Keys, F. Kesbeke, P.J. Wijngaarden, A. Monteiro, V. French, and S.B. Carroll. 1996. Development, plasticity and evolution of butterfly eyespot patterns. *Nature.* 384:236–242.

Brand, A.H., and N. Perrimon. 1993. Targeted gene expression as a means of altering cell fates and generating dominant phenotypes. *Development.* 118:401–415.

Burridge, K., and K. Wennerberg. 2004. Rho and rac take center stage. *Cell.* 116: 167–179.

Castrillon, D.H., and S.A. Wasserman. 1994. Diaphanous is required for cytokinesis in *Drosophila* and shares domains of similarity with the products of the limb deformity gene. *Development.* 120:3367–3377.

Celniker, S.E., D.A. Wheeler, B. Kronmiller, J.W. Carlson, A. Halpern, S. Patel, M. Adams, M. Champe, S.P. Dugan, E. Frise, et al. 2002. Finishing a whole-genome shotgun: release 3 of the *Drosophila melanogaster* euchromatic genome sequence. *Genome Biol.* 3:RESEARCH0079.

D'Avino, P.P., and C.S. Thummel. 1998. *crooked legs* encodes a family of zinc finger proteins required for leg morphogenesis and ecdysone-regulated gene expression during *Drosophila* metamorphosis. *Development.* 125:1733–1745.

D'Avino, P.P., S. Crispi, L.C. Polito, and M. Furia. 1995. The role of the *BR-C* locus on the expression of genes located at the ecdysone-regulated 3C puff of *Drosophila melanogaster*. *Mech. Dev.* 49:161–171.

Deak, P., M.M. Omar, R.D. Saunders, M. Pal, O. Komonyi, J. Szidonya, P. Maroy, Y. Zhang, M. Ashburner, P. Benos, et al. 1997. P-element insertion alleles of essential genes on the third chromosome of *Drosophila melanogaster*: correlation of physical and cytogenetic maps in chromosomal region 86E-87F. *Genetics.* 147:1697–1722.

Di Cunto, F., E. Calautti, J. Hsiao, L. Ong, G. Topley, E. Turco, and G.P. Dotto. 1998. Citron rho-interacting kinase, a novel tissue-specific ser/thr kinase encompassing the Rho-Rac-binding protein Citron. *J. Biol. Chem.* 273:29706–29711.

Di Cunto, F., S. Imarisio, E. Hirsch, V. Broccoli, A. Bulfone, A. Migheli, C. Atzori, E. Turco, R. Triolo, G.P. Dotto, et al. 2000. Defective neurogenesis in citron kinase knockout mice by altered cytokinesis and massive apoptosis. *Neuron.* 28:115–127.

Di Cunto, F.D., S. Imarisio, P. Camera, C. Boitani, F. Altruda, and L. Silengo. 2002. Essential role of citron kinase in cytokinesis of spermatogenic precursors. *J. Cell Sci.* 115:4819–4826.

Drechsel, D.N., A.A. Hyman, A. Hall, and M. Glotzer. 1997. A requirement for Rho and Cdc42 during cytokinesis in Xenopus embryos. *Curr. Biol.* 7:12–23.

Eda, M., S. Yonemura, T. Kato, N. Watanabe, T. Ishizaki, P. Madaule, and S. Narumiya. 2001. Rho-dependent transfer of Citron-kinase to the cleavage furrow of dividing cells. *J. Cell Sci.* 114:3273–3284.

Fehon, R.G., I.A. Dawson, and S. Artavanis-Tsakonas. 1994. A *Drosophila* homologue of membrane-skeleton protein 4.1 is associated with septate junctions and is encoded by the coracle gene. *Development.* 120:545–557.

Field, C., R. Li, and K. Oegema. 1999. Cytokinesis in eukaryotes: a mechanistic comparison. *Curr. Opin. Cell Biol.* 11:68–80.

Field, C.M., and B.M. Alberts. 1995. Anillin, a contractile ring protein that cycles from the nucleus to the cell cortex. *J. Cell Biol.* 131:165–178.

Gatti, M., and B.S. Baker. 1989. Genes controlling essential cell-cycle functions in *Drosophila melanogaster*. *Genes Dev.* 3:438–453.

Giansanti, M.G., S. Bonaccorsi, and M. Gatti. 1999. The role of anillin in meiotic cytokinesis of *Drosophila* males. *J. Cell Sci.* 112:2323–2334.

Giet, R., and D.M. Glover. 2001. *Drosophila* Aurora B kinase is required for histone H3 phosphorylation and condensin recruitment during chromosome condensation and to organize the central spindle during cytokinesis. *J. Cell Biol.* 152:669–682.

Giordano, E., R. Rendina, I. Peluso, and M. Furia. 2002. RNAi triggered by symmetrically transcribed transgenes in *Drosophila melanogaster*. *Genetics.* 160: 637–648.

Glotzer, M. 2001. Animal cell cytokinesis. *Annu. Rev. Cell Dev. Biol.* 17:351–386.

Gonzalez, C., and D.M. Glover. 1993. Techniques for studying mitosis in *Dro-*

sophila. *In* The Cell Cycle: A Practical Approach. P. Fantes and R. Brooks, editors. IRL Press, Oxford. 163–168.

Gu, Y., and D.A. Williams. 2002. RAC2 GTPase deficiency and myeloid cell dysfunction in human and mouse. *J. Pediatr. Hematol. Oncol.* 24:791–794.

Hakeda-Suzuki, S., J. Ng, J. Tzu, G. Dietzl, Y. Sun, M. Harms, T. Nardine, L. Luo, and B.J. Dickson. 2002. Rac function and regulation during *Drosophila* development. *Nature.* 416:438–442.

Ikebe, M., and D.J. Hartshorne. 1985. Phosphorylation of smooth muscle myosin at two distinct sites by myosin light chain kinase. *J. Biol. Chem.* 260: 10027–10031.

Jantsch-Plunger, V., P. Gonczy, A. Romano, H. Schnabel, D. Hamill, R. Schnabel, A.A. Hyman, and M. Glotzer. 2000. CYK-4: a Rho family gtpase activating protein (GAP) required for central spindle formation and cytokinesis. *J. Cell Biol.* 149:1391–1404.

Jordan, P., and R. Karess. 1997. Myosin light chain-activating phosphorylation sites are required for oogenesis in *Drosophila*. *J. Cell Biol.* 139:1805–1819.

Kitamura, T., T. Kawashima, Y. Minoshima, Y. Tonozuka, K. Hirose, and T. Nosaka. 2001. Role of MgcRacGAP/Cyk4 as a regulator of the small GTPase Rho family in cytokinesis and cell differentiation. *Cell Struct. Funct.* 26: 645–651.

Kosako, H., T. Yoshida, F. Matsumura, T. Ishizaki, S. Narumiya, and M. Inagaki. 2000. Rho-kinase/ROCK is involved in cytokinesis through the phosphorylation of myosin light chain and not ezrin/radixin/moesin proteins at the cleavage furrow. *Oncogene.* 19:6059–6064.

Lundquist, E.A., P.W. Reddien, E. Hartwieg, H.R. Horvitz, and C.I. Bargmann. 2001. Three *C. elegans* Rac proteins and several alternative Rac regulators control axon guidance, cell migration and apoptotic cell phagocytosis. *Development.* 128:4475–4488.

Madaule, P., T. Furuyashiki, T. Reid, T. Ishizaki, G. Watanabe, N. Morii, and S. Narumiya. 1995. A novel partner for the GTP-bound forms of rho and rac. *FEBS Lett.* 377:243–248.

Madaule, P., M. Eda, N. Watanabe, K. Fujisawa, T. Matsuoka, H. Bito, T. Ishizaki, and S. Narumiya. 1998. Role of citron kinase as a target of the small GTPase Rho in cytokinesis. *Nature.* 394:491–494.

Madaule, P., T. Furuyashiki, M. Eda, H. Bito, T. Ishizaki, and S. Narumiya. 2000. Citron, a Rho target that affects contractility during cytokinesis. *Microsc. Res. Tech.* 49:123–126.

Minestrini, G., E. Mathe, and D.M. Glover. 2002. Domains of the Pavarotti kinesin-like protein that direct its subcellular distribution: effects of mislocalisation on the tubulin and actin cytoskeleton during *Drosophila* oogenesis. *J. Cell Sci.* 115:725–736.

Minoshima, Y., T. Kawashima, K. Hirose, Y. Tonozuka, A. Kawajiri, Y.C. Bao, X. Deng, M. Tatsuka, S. Narumiya, W.S. May Jr., et al. 2003. Phosphorylation by aurora B converts MgcRacGAP to a RhoGAP during cytokinesis. *Dev. Cell.* 4:549–560.

Mishima, M., S. Kaitna, and M. Glotzer. 2002. Central spindle assembly and cytokinesis require a kinesin-like protein/RhoGAP complex with microtubule bundling activity. *Dev. Cell.* 2:41–54.

Muris, D.F., T. Verschoor, N. Divecha, and R.J. Michalides. 2002. Constitutive active GTPases Rac and Cdc42 are associated with endoreplication in PAE cells. *Eur. J. Cancer.* 38:1775–1782.

Nagahashi, S., T. Mio, N. Ono, T. Yamada-Okabe, M. Arisawa, H. Bussey, and H. Yamada-Okabe. 1998. Isolation of CaSLN1 and CaNIK1, the genes for osmosensing histidine kinase homologues, from the pathogenic fungus *Candida albicans*. *Microbiology.* 144:425–432.

Neufeld, T.P., and G.M. Rubin. 1994. The *Drosophila* peanut gene is required for cytokinesis and encodes a protein similar to yeast putative bud neck filament proteins. *Cell.* 77:371–379.

Ng, J., T. Nardine, M. Harms, J. Tzu, A. Goldstein, Y. Sun, G. Dietzl, B.J. Dickson, and L. Luo. 2002. Rac GTPases control axon growth, guidance and branching. *Nature.* 416:442–447.

O'Connell, C.B., S.P. Wheatley, S. Ahmed, and Y.L. Wang. 1999. The small GTP-binding protein rho regulates cortical activities in cultured cells during division. *J. Cell Biol.* 144:305–313.

Ozaki, K., K. Tanaka, H. Imamura, T. Hihara, T. Kameyama, H. Nonaka, H. Hirano, Y. Matsuura, and Y. Takai. 1996. Rom1p and Rom2p are GDP/GTP exchange proteins (GEPs) for the Rho1p small GTP binding protein in *Saccharomyces cerevisiae*. *EMBO J.* 15:2196–2207.

Paddy, M.R., A.S. Belmont, H. Saumweber, D.A. Agard, and J.W. Sedat. 1990. Interphase nuclear envelope lamins form a discontinuous network that interacts with only a fraction of the chromatin in the nuclear periphery. *Cell.* 62: 89–106.

Piekny, A.J., and P.E. Mains. 2002. Rho-binding kinase (LET-502) and myosin phosphatase (MEL-11) regulate cytokinesis in the early *Caenorhabditis elegans* embryo. *J. Cell Sci.* 115:2271–2282.

Prokopenko, S.N., A. Brumby, L. O'Keefe, L. Prior, Y. He, R. Saint, and H.J. Bellen. 1999. A putative exchange factor for Rho1 GTPase is required for initiation of cytokinesis in *Drosophila*. *Genes Dev.* 13:2301–2314.

Prokopenko, S.N., R. Saint, and H.J. Bellen. 2000. Untying the Gordian knot of cytokinesis: role of small G proteins and their regulators. *J. Cell Biol.* 148: 843–848.

Rebecchi, M.J., and S. Scarlata. 1998. Pleckstrin homology domains: a common fold with diverse functions. *Annu. Rev. Biophys. Biomol. Struct.* 27:503–528.

Robinson, D.N., and J.A. Spudich. 2000. Towards a molecular understanding of cytokinesis. *Trends Cell Biol.* 10:228–237.

Somers, W.G., and R. Saint. 2003. A RhoGEF and Rho family GTPase-activating protein complex links the contractile ring to cortical microtubules at the onset of cytokinesis. *Dev. Cell.* 4:29–39.

Somma, M.P., B. Fasulo, G. Cenci, E. Cundari, and M. Gatti. 2002. Molecular dissection of cytokinesis by RNA interference in *Drosophila* cultured cells. *Mol. Biol. Cell.* 13:2448–2460.

Strutt, D.I., U. Weber, and M. Mlodzik. 1997. The role of RhoA in tissue polarity and Frizzled signalling. *Nature.* 387:292–295.

Swan, K.A., A.F. Severson, J.C. Carter, P.R. Martin, H. Schnabel, R. Schnabel, and B. Bowerman. 1998. *cyk-1*: a *C. elegans* FH gene required for a late step in embryonic cytokinesis. *J. Cell Sci.* 111:2017–2027.

Tatsumoto, T., X. Xie, R. Blumenthal, I. Okamoto, and T. Miki. 1999. Human ECT2 is an exchange factor for Rho GTPases, phosphorylated in G2/M phases, and involved in cytokinesis. *J. Cell Biol.* 147:921–928.

Toure, A., O. Dorseuil, L. Morin, P. Timmons, B. Jegou, L. Reibel, and G. Gacon. 1998. MgcRacGAP, a new human GTPase-activating protein for Rac and Cdc42 similar to *Drosophila* rotundRacGAP gene product, is expressed in male germ cells. *J. Biol. Chem.* 273:6019–6023.

Watanabe, N., P. Madaule, T. Reid, T. Ishizaki, G. Watanabe, A. Kakizuka, Y. Saito, K. Nakao, B.M. Jockusch, and S. Narumiya. 1997. p140mDia, a mammalian homolog of *Drosophila* diaphanous, is a target protein for Rho small GTPase and is a ligand for profilin. *EMBO J.* 16:3044–3056.

Winter, C.G., B. Wang, A. Ballew, A. Royou, R. Karess, J.D. Axelrod, and L. Luo. 2001. *Drosophila* Rho-associated kinase (Drok) links Frizzled-mediated planar cell polarity signaling to the actin cytoskeleton. *Cell.* 105:81–91.

Yamashiro, S., G. Totsukawa, Y. Yamakita, Y. Sasaki, P. Madaule, T. Ishizaki, S. Narumiya, and F. Matsumura. 2003. Citron kinase, a Rho-dependent kinase, induces di-phosphorylation of regulatory light chain of myosin II. *Mol. Biol. Cell.* 14:1745–1756.

Yoshizaki, H., Y. Ohba, K. Kurokawa, R.E. Itoh, T. Nakamura, N. Mochizuki, K. Nagashima, and M. Matsuda. 2003. Activity of Rho-family GTPases during cell division as visualized with FRET-based probes. *J. Cell Biol.* 162:223–232.